HHS Public Access

Author manuscript

Cytoskeleton (Hoboken). Author manuscript; available in PMC 2021 July 06.

Published in final edited form as:

Cytoskeleton (Hoboken). 2020 July ; 77(7): 277–291. doi:10.1002/cm.21622.

Investigating the impact of the phosphorylation status of tyrosine residues within the TACC domain of TACC3 on microtubule behavior during axon growth and guidance

Burcu Erdogan[1,2], **Riley M. St. Clair**[3], **Garrett M. Cammarata**[1], **Timothy Zaccaro**[1], **Bryan A. Ballif**[3], **Laura Anne Lowery**[4,*]

[1]Boston College Department of Biology, 140 Commonwealth Avenue, Chestnut Hill, MA, 02467, USA

[2]Harvard Department of Stem Cell and Regenerative Biology, 7 Divinity Avenue, Cambridge, MA, 02138, USA

[3]Department of Biology, University of Vermont, 109 Carrigan Drive, 120A Marsh Life Sciences, Burlington, VT, 05405, USA

[4]Department of Medicine, Boston University Medical Center, 650 Albany St, Boston, MA, 02118, USA

Abstract

Axon guidance is a critical process in forming the connections between a neuron and its target. The growth cone steers the growing axon towards the appropriate direction by integrating extracellular guidance cues and initiating intracellular signal transduction pathways downstream of these cues. The growth cone generates these responses by remodeling its cytoskeletal components. Regulation of microtubule dynamics within the growth cone is important for making guidance decisions. TACC3, as a microtubule plus-end binding protein, modulates microtubule dynamics during axon outgrowth and guidance. We have previously shown that *Xenopus laevis* embryos depleted of TACC3 displayed spinal cord axon guidance defects, while TACC3-overexpressing spinal neurons showed increased resistance to Slit2-induced growth cone collapse. Tyrosine kinases play an important role in relaying guidance signals to downstream targets during pathfinding events via inducing tyrosine phosphorylation. Here, in order to investigate the mechanism behind TACC3-mediated axon guidance, we examined whether tyrosine residues that are present in TACC3 have any role in regulating TACC3's interaction with microtubules or during axon outgrowth and guidance behaviors. We find that the phosphorylatable tyrosines within the TACC domain are important for the microtubule plus-end tracking behavior of TACC3. Moreover, TACC domain phosphorylation impacts axon outgrowth dynamics such as growth length and growth persistency. Together, our results suggest that tyrosine phosphorylation of TACC3 affects TACC3's microtubule plus-end tracking behavior as well as its ability to mediate axon growth dynamics in cultured embryonic neural tube explants.

[*]Corresponding author: Laura Anne Lowery (lalowery@bu.edu).

Keywords

Axon guidance; growth cone; microtubule; +TIPs; TACC3; Abelson kinase; tyrosine phosphorylation

1 | INTRODUCTION

Regulation of cytoskeletal dynamics within the growth cone is essential for growth cone motility and navigation as the axon travels to its target (reviewed in Lowery and Van Vactor 2008). Guidance molecules that the growth cone encounters during its trip can act as repellent or attractant depending on the time, location and the signal composition of the environment that the growth cone passes. Integration and interpretation of these signals relies on signaling cascades that are initiated downstream of guidance cue receptors which will ultimately converge upon cytoskeletal elements for their rearrangements and control of growth cone motility.

Guidance signals are not homogeneously presented to the growth cone *in vivo*. While the growth cone might be exposed to repellent signals on one side, it can be exposed to attractant signals on the other side, which necessitates the asymmetric reorganization of the underlying cytoskeleton. In order to manage this asymmetric regulation, signals received by guidance cue receptors must be processed locally and immediately downstream of the site where the signal is received without necessarily leading to a global response. For example, repulsive guidance cues can cause a global growth cone collapse when they are bath-applied, whereas their local application causes collapse on the side that the protein is received, which results in growth cone steering away from the source of the signal (Buck and Zheng, 2002).

The interaction between guidance cue receptors and downstream targets is required for the growth cone's directional movement. Microtubule plus-end tracking proteins (+TIPs), due to their localization close to the growth cone periphery, are potential targets for guidance signals. Their interaction with microtubules at the plus-ends is important for regulating microtubule growth dynamics and coordination of signal exchange between the growth cone periphery and the central domain, which is critical to the growth cone's directional movement.

The interaction between +TIPs and microtubules can be modulated by guidance signals and their downstream intracellular signaling events. Phosphorylation of +TIPs is one such event that has been shown to modulate +TIP affinity for microtubules. For example, the affinity of CLASP for microtubules has been shown to be regulated differentially in migrating epithelial cells (Kumar et al., 2009; Wittmann and Waterman-Storer, 2005) as well as growth cones (Hur et al., 2011) depending on its phosphorylation status by GSK3 kinase. Increased microtubule lattice binding activity of CLASP, as a result of GSK3 inhibition, results in axon growth inhibition through inhibition of microtubule advance into the growth cone periphery. On the other hand, plus-end binding of CLASP, as a result of GSK3 activity, promotes axon outgrowth via stabilization of microtubules (Hur et al., 2011). In addition to GSK3, CLASP has also been identified as a direct target of Abelson (Abl) tyrosine kinase (Engel et al., 2014; Lee et al., 2004). Further examination of the interaction between CLASP and Abl in

Xenopus spinal neurons identified CLASP as a target for Abl phosphorylation and showed that phosphorylation can affect CLASP localization in neuronal growth cones (Engel et al., 2014).

Similar to CLASP, several +TIPs have been implicated to be involved in regulation of microtubule dynamics during directional movement of cells and growth cones (Bearce et al., 2015). However, only a few of them have been studied and implicated as a target for guidance cue-initiated intracellular signals (Bearce et al., 2015). We have previously characterized a microtubule plus-end tracking function for TACC3 in neuronal growth cones and showed that TACC3 overexpression enhances microtubule growth dynamics and promotes axon outgrowth (Nwagbara et al., 2014). Additionally, we have proposed a function for TACC3 during axon guidance. Reducing levels of TACC3 resulted in disorganized axon elongation of neural tube neurons in *Xenopus laevis* embryos and its overexpression mitigated growth cone collapse induced by bath-applied Slit2 in cultured *Xenopus laevis* neural tube explants (Erdogan et al., 2017). To further investigate the mechanism by which TACC3 overexpression exerts this opposing role against Slit2 activity, we became interested in looking at potential phosphorylation events that might target TACC3. Tyrosine phosphorylation has been implicated to be an important signaling event in axon guidance. Our previous studies highlighted a possible genetic interaction network between TACC3, its microtubule polymerase interactor XMAP215, and Abelson tyrosine kinase (Abl) (Lowery et al., 2010). Thus, we became interested in testing whether TACC3 could be a target for tyrosine kinases in particular Abl kinase downstream of Slit2 and whether its tyrosine phosphorylation status would alter the interaction of TACC3 with microtubules as well as its impact on axon outgrowth and guidance.

2 | RESULTS

2.1 | Abelson kinase induces phosphorylation of TACC3

To investigate whether Abelson tyrosine kinase (Abl) induces phosphorylation of TACC3, we co-expressed GFP-TACC3 and Abl in HEK293 cells. We immunoprecipitated GFP-TACC3 with a GFP antibody and performed Western blot analysis with a phospho-tyrosine specific antibody, 4G10. We found that TACC3 receives tyrosine phosphorylation when co-expressed with Abl (Figure 1a, lane 4). Phosphorylation of TACC3 was only observed when it was co-expressed with Abl (Figure 1a, lane 3 vs lane 4). Additionally, this phosphorylation specifically happened with the tyrosine kinase Abl, since Fyn, which is another tyrosine kinase, did not induce TACC3 tyrosine phosphorylation (Figure 1a, lane 6). Although we did not determine whether the induced tyrosine phosphorylation was a result of direct interaction between Abl and TACC3, our data show that Abl expression can induce phosphorylation of tyrosine residues on TACC3.

To study the role of TACC3 phosphorylation, we next wanted to identify the tyrosine residues that are targeted by Abl. HEK293 cells were transfected with expression plasmids encoding GFP-TACC3 alone or with Abl. TACC3 was then immunopurified using anti-GFP from cell extracts of each group and subjected to SDS-PAGE and coomassie staining. The region corresponding to the molecular weight of GFP-TACC3 (180 kDa) was excised and subjected to in-gel tryptic digestion. Tryptic peptides were analyzed using LC-MS/MS, and

a SEQUEST search identified 4 tyrosine residues on TACC3 that were phosphorylated when co-expressed with Abl: two (Y759, Y762) in the conserved TACC domain, the domain that is responsible for microtubule plus-end binding, and two (Y608, Y628) outside of the TACC domain (Figure 1b, Supplementary Figures 1-6). These phosphorylation events only occurred when Abl was co-expressed with TACC3. Three additional tyrosine residues were detected, however they were not found to be phosphorylated: two (Y130 and Y320) outside the TACC domain and one (Y725) within the TACC domain.

To assess the importance of the phosphorylated tyrosine residues, we generated single and combinatorial phospho-null mutants of TACC3 by substituting the four tyrosine residues found to be phosphorylated with alanine or phenylalanine. However, neither single nor combinatorial phospho-null mutations caused a reduction in tyrosine phosphorylation levels, determined by Western blot analysis (Supplementary Figure 7a-d). Moreover, all of the single and combinatorial mutants were still able to track microtubule plus-ends (Figure 1c-h, Supplemental Movies 1-6). This initial examination suggests that other tyrosine residues (besides those identified by mass-spec) might also be phosphorylated in TACC3 and thus contribute to the overall phospho-tyrosine signal detected by Western blot. Indeed, there are four additional tyrosine residues in TACC3 that were not detected by the mass spectrometry, including three (Y832, Y846, Y857) in the TACC domain and one (Y428) outside of the TACC domain.

2.2 | Tyrosine phospho-null mutations impair the localization of the TACC domain at microtubule plus-ends in growth cones and mesenchymal cells

Since none of the TACC3 phospho-null mutants based on mass-spec-identified tyrosine residues showed a reduction in phosphorylation signal, and they were all still able to localize to microtubules, we decided to examine other tyrosine residues within TACC3, in an attempt to identify the source of tyrosine signal we observed with Western blot. The full-length TACC3 possesses a total of 11 tyrosine residues throughout the entire protein. Six of these tyrosine residues (Y725, Y759, Y762, Y832, Y846, Y857) are in the TACC domain (aa715-aa931), one (Y130) is in the N-terminal domain (aa1-aa133), and four (Y320, Y428, Y608, Y628) are in the middle domain (aa134-aa634) (Figure 2a).

The C-terminal TACC domain of the TACC3 protein shows high sequence similarity among vertebrates as well as among other TACC family members (Peset and Vernos, 2008) (Supplementary Figure 10). Moreover, the TACC domain is the portion of the TACC3 protein that is responsible for its microtubule plus-end tracking behavior (Nwagbara et al., 2014) and also for interacting with the microtubule polymerase XMAP215 (Mortuza et al., 2014). Therefore, we decided to specifically investigate the importance of tyrosine residues within the TACC domain, to determine whether they might be contributing to the Abl-induced phosphorylation we observed earlier. To investigate this, we mutated all six of the tyrosine residues within the TACC domain to phenylalanine (Figure 2a) and tested these mutants for their phosphorylation status. (Note that in our mass spec experiment, Y759 and Y762 had been phosphorylated, Y725 had not been present but not phosphorylated, while Y832, Y846, and Y857 peptides had not been detected at all.) Surprisingly, despite lacking a phosphorylatable tyrosine with the TACC sequence, GFP-TACC phospho-null mutants

showed similar phospho-tyrosine signals compared to the wild-type TACC domain, as verified with Western blot (Supplementary Figure 8a, lane 5-6). Since there were no tyrosines left in the TACC domain, the only other source that might have contributed to the observed Western blot signal was GFP. Therefore, we performed a Western blot for the GFP tag alone with a phospho-tyrosine specific antibody, and we found that GFP was indeed getting phosphorylated specifically in the presence of Abl kinase (Supplementary Figure 8b-c, lane 4-5). Thus, GFP itself was probably contributing to the overall signal that we obtained with the GFP-tagged TACC constructs previously. However, while Abl-induced phosphorylation of GFP muddled the Western blot results, we still had previously determined that tyrosine residues of TACC3 were indeed being phosphorylated as a result of Abl signaling, as determined by mass-spec and Western blot. Therefore, for the rest of the study, we decided to pursue whether tyrosine phosphorylation directly impacted the ability of the TACC domain to bind microtubules.

When we examined whether TACC protein with tyrosine phospho-null mutations (TACC 6xYF) could still localize to microtubules, we found that both full-length TACC3 phospho-null mutants (data not shown) and TACC domain-only phospho-null mutants showed changes in their microtubule localization (Figure 2b-e, Supplemental Movie 7-8). In both neuronal growth cones (and mesenchymal cells, not shown) isolated from *Xenopus* embryos, TACC phospho-null mutants showed less localization along microtubules, determined by line-scan averages of fluorescent intensities obtained from microtubule plus-ends (Figure 2f). The TACC phospho-null mutant remained cytoplasmic in 80% of the growth cones and showed microtubule localization in 20% of the growth cones examined, while wild-type TACC localized at microtubule plus-ends in 93% of growth cones (Figure 2g). We also confirmed protein expression levels by Western blot and showed that the GFP-TACC mutant expression was comparable to wild-type GFP-TACC (Figure 2h). These data suggest that retaining phosphorylatable tyrosines within the TACC domain is important for TACC microtubule localization.

2.3 | TACC tyrosine phospho-null mutant-expressing axons grow less persistently, thereby resulting in shorter axons compared to TACC wild-type-expressing axons

We have previously shown that TACC3 binding to microtubules is critical for promoting axon outgrowth (Nwagbara et al., 2014). To test whether phosphorylation of the TACC domain is important in regulating axon outgrowth parameters, we measured the length of axons in cultured *Xenopus laevis* neural tube explants expressing either TACC wild-type (wt) protein or TACC phospho-null mutant protein. While expression of TACC wt led to formation of longer axons, expression of the TACC phospho-null mutant (0.86 ± 0.04, N= 155) was unable to promote increased axon outgrowth, and instead, showed a 17% reduction in axon length compared to controls (1.00 ± 0.03, N=277) and a 34% reduction compared to TACC wt (1.15± 0.06, N=199) (Figure 3a).

To further assess the difference in axon length between the neurons expressing TACC wt and the phospho-null mutant, we measured axon outgrowth velocities. Interestingly, despite the fact that phospho-null mutant-expressing axons were not as long as TACC wt-expressing axons, we found only minor (insignificant) differences in outgrowth velocity. The average

normalized axon forward movement velocity was 8% faster in TACC phospho-null mutant conditions (1.10± 0.03 N=172, **p=0.0082) compared to controls (1.00 ± 0.02 N=198) and only 4% slower, compared to TACC wt (1.13 ± 0.03 N=217, not significant p=0.3). Average outgrowth velocity in TACC wt-expressing axons, on the other hand was 10% faster compared to control axons (Figure 3b). Our data suggests that TACC phospho-null mutant-expressing axons grow at similar rates to the TACC wt-expressing axons, suggesting that the reduced axon length in the phospho-null condition could be due to another parameter of axon growth other than outgrowth velocity.

To further investigate this, we also tracked other growth behaviors of axons and recorded the number of frames that they moved forward, paused and/or retracted over the course of 4 hour long time-lapse imaging (Figure 3c, Supplemental Movie 9-10, intervals were every 5 minutes). We found that TACC phospho-null mutant-expressing axons (69.61 ± 1.77, N=168) spent 18% less time moving forward compared to controls (82.30 ± 1.5, N=183, ***p<0.0001) and 12% less compared to TACC wt (78.20 ± 1.43, N=218, ***p<0.0001) (Figure 3d, green dots). Additionally, TACC phospho-null mutant axons (20.20 ± 1.150, N=168) spent 42% more time pausing compared to controls (11.67 ± 1.00, N=183, ***p<0.0001) and 27% more compared to TACC wt 14.67 ± 0.97, N=218, ***p=0.0003) (Figure 3d, orange dots). They also retracted more frequently: 39% compared to controls (6.125 ± 0.89 N=183, **p=0.0043) and 30% compared to TACC wt (7.098 ± 0.67 N=218, *p=0.0132) (Figure 3d, red dots, Supplemental Movie 11).

In addition to pause and frequency rates, we also examined the directness of axon outgrowth. The still images of neural tube explants that were used to measure axon length show the final displacement of an axon. However, axons do not necessarily follow a linear trajectory as they grow. In fact, they often spend time wandering, which is part of their exploratory behavior. Therefore, the directness of outgrowth can be determined by dividing the displacement distance by the total distance traveled (Figure 3e). We found that TACC phospho-null mutant expressing-axons (0.5353 ± 0.02, N=179) grew 12% less directly compared to TACC wt-expressing axons (0.6012 ± 0.02, N=195) and 17% less compared to control axons (0.6313 ± 0.02, N=192, Figure 3f).

These data suggest that while axon outgrowth speed is not affected by TACC tyrosine phospho-null mutations, growth persistency, which is determined by pause and retraction frequency, as well as growth directionality, both seem to be impaired in TACC phospho-null mutant-expressing axons. Thus, this could explain the shorter axon length that we observed in TACC phospho-null mutant-expressing neural tube explants.

2.4 | TACC wild-type and tyrosine phospho-null mutant-expressing growth cones display increased numbers of filopodia that contain microtubules

Axons of neurons expressing the TACC phospho-null mutant stop and retract more frequently compared to those expressing wild-type TACC. Additionally, we observe that their growth is less directed compared to TACC wild-type and controls. An inverse correlation between growth cone advance rate and growth cone size has been reported previously (Ren and Suter, 2016). Therefore, we became interested in examining the growth cone size, along with other morphological features, to see whether increased pause and

retraction rates in TACC phospho-null mutant-expressing growth cones might also occur alongside changes in growth cone morphology.

We initially examined the growth cone area, filopodia length, and filopodia number in cultured neural tube explants that were fixed and stained for microtubules (tubulin) and actin (phalloidin), followed by high resolution Structured Illumination Microscopy (SIM) imaging. We found no significant difference in any of the morphological features examined (Figure 4a-c). The average growth cone area of TACC phospho-null mutant-expressing growth cones (406.5 ± 37.17 μm, N=88, p=0.6) was 13% smaller than control (432.6 ± 39.62 μm, N=77) and 6% larger than TACC wt (382.5 ± 30.17 μm, N=94, n.s. p=0.6) (Figure 4a). The average filopodia number did not differ across conditions either (n.s. p=0.4). TACC phospho-null mutant growth cones had an average of 6.9 ± 0.41 N=93 filopodia, which was 10% less than control growth cones (7.6 ± 0.45 N=89) while TACC wt had 9% fewer filopodia than control (7.0 ± 0.38 N=101) (Figure 4b). The average filopodia length in TACC phospho-null mutant growth cones was 17.03 ± 0.84μm, N=113, while it was 16.07 ± 0.77 μm, N=119 in control growth cones, and 15.96 ± 0.51 μm, N=126 in TACC wt expressing growth cones (Figure 4c).

However, while average filopodia number was similar among conditions, the number of filopodia that contained microtubules was found to be significantly higher in the TACC wt and phospho-null mutant-expressing growth cones. Almost 30% of the filopodia had microtubules in the TACC phospho-null mutant growth cones (29.13 ± 2.932 percent of total filopodia examined, N=82), which is 63% more than control growth cones (10.92 ± 2.011 percent of total filopodia examined, N=90, ***p<0.0001), that had only 11% of their filopodia invaded by microtubules. TACC wt-expressing growth cones also had a greater number of filopodia with microtubules (25.82 ± 2.446 N=92, ***p<0.0001) compared to controls. While not significant, TACC phospho-null growth cones had 11% more filopodia with microtubules compared to TACC wt (Figure 4g). Thus, it appears that overexpression of the TACC domain, regardless of its phosphorylation status, leads to an increased number of microtubules that penetrate into filopodia. Although not significant, the percentage of filopodia with microtubules is slightly higher in TACC phospho-null mutant-overexpressing growth cones compared to TACC wild-type expressing growth cones which may directly or indirectly contribute to increased pausing and retraction rates of axons observed with TACC phospho-null mutant axons.

2.5 | TACC domain-expressing axons are more responsive to repellent guidance signals

We previously tested TACC3 function downstream of Slit2 and found that growth cones overexpressing TACC3 were more resilient to bath-applied Slit2-induced growth cone collapse compared to control growth cones (Erdogan et al., 2017). While bath application of guidance proteins is useful to test how manipulation of protein levels would alter the growth cone's reaction to an applied guidance molecule, it does not convey information regarding the ability of the growth cone to make guidance choices such as steering. In order to test that, we utilized an approach where the repellent guidance protein Ephrin-A5 was coated on a glass coverslip in zigzag patterns and neural tube explants were cultured on top of these cue-coated coverslips. After 12-18 h of culturing, explants were fixed and stained for tubulin

and actin to examine axon responsiveness to Ephrin-A5. The responsiveness was scored based on how many of the axons that grew out from the given explant preferred to stay on the Ephrin-A5-free (growth permissive) surface versus how many of them crossed that barrier and grew on the Ephrin-A5 (non-permissive) surface.

We found that control neural tube explants (Figure 5a), composed of a heterogeneous population of neurons, did not show a preference towards a particular surface and grew axons on both permissive (Ephrin-A5 free, dark stripes) and non-permissive (Ephrin-A5, green stripes) surfaces equally (Figure 5d; Control - off, 50.01 ± 2.93 N=55; Control- on, 49.99 ± 2.93, respectively, n.s, p=0.9). However, TACC w- overexpressing neural tube explants (Figure 5b) showed a preference for the permissive surfaces, as they grew 25% more axons on permissive surfaces (Figure 5d; 57.18 ± 2.68 N=62, TACC wt – off, ***p=0.0002) compared to the Ephrin-A5 coated surface (TACC wt - on, 42.82 ± 2.68 N=62). TACC phospho-null mutant-expressing axons (Figure 5c), on the other hand, showed a slightly stronger preference for the permissive surface, as they grew 41.3% more axons on the permissive surface (Figure 5d; TACC mut - off, 63.02 ± 3.03 N=42, ***p<0.0001) compared to the Ephrin-A5 coated non-permissive surface (TACC mut - on, 36.98 ± 3.03 N=42). Together, these data suggest that axons overexpressing TACC domain are less able to grow on the Ephrin surface and are thus more responsive to the Ephrin-A5 repellent guidance cue activity. Additionally, responsiveness of axons to Ephrin is not necessarily affected by the phosphorylation status of TACC domain, as the difference between TACC wild-type and TACC phospho-null mutant expressing axons was not significantly different.

3 | DISCUSSION

3.1 | Abelson kinase induces phosphorylation of TACC3

In this study, we sought to examine the impact of TACC3 tyrosine phosphorylation on its interaction with microtubules and regulation of axon outgrowth and guidance. We showed that co-expressing TACC3 with Abelson kinase (Abl) in HEK293 cells induces TACC3 tyrosine phosphorylation, as evident by the phospho-tyrosine signal we obtained by Western blot. Our Western blot analysis also showed that phosphorylation of TACC3 happened only in the presence of Abelson, as we did not observe any phospho-tyrosine signal when TACC3 was expressed alone or with Fyn, which is another tyrosine kinase (Figure 1a). Mass-spectrometry analysis of GFP-TACC3 that was co-expressed with Abl in HEK 293 cells identified phosphorylated tyrosine residues as to be potential targets for Abl tyrosine kinase (Supplementary Figures 1-6).

Interestingly, creating single or combinatorial phospho-null mutations at those tyrosine residues that we identified as potential targets for Abl did not show any changes in phospho-tyrosine signal levels observed with Western blot. In an attempt to identify the source of tyrosine phosphorylation, we tested other tyrosine residues and focused specifically on the ones in the TACC domain, positioned at the C-terminal of TACC3 and responsible for microtubule plus-end tracking and interaction with its well-studied partner, microtubule polymerase XMAP215. The TACC domain possesses 6 tyrosine residues with two of them (Y759 and Y762, aa location given based on full length protein) identified as Abl targets from the mass-spec analysis and three of them (Y832, Y846 and Y857) predicted as putative

targets for Abl via *in silico* analysis. Intriguingly, mutating all these tyrosines into non-phosphorylatable phenylalanine did not cause any reduction in the phospho-tyrosine signal level as evident by the Western blot (Supplementary Figure 8a-b). In spite of the lack of any tyrosines in the TACC domain, it was interesting to see that there was still a phospho-tyrosine signal in the Western blot. The only possible source of phosphorylatable tyrosine was GFP that is tagged to the TACC domain. Tyrosine phosphorylation of GFP has not been reported previously, to our knowledge, nor does *in silico* phosphorylation prediction identify any sites by which kinases might target GFP. However, expression of GFP with Abl clearly showed a strong phospho-tyrosine signal (Supplementary Figure 8b-c, lane 4) suggesting that GFP might be partially contributing to the phospho-tyrosine signal that we had been observing in GFP-TACC.

3.2 | Tyrosine residues within the TACC domain are important for TACC localization to microtubules

The impact of phosphorylation on the interaction between +TIPs and microtubules has been studied for several +TIPs, such as CLASP (Hur et al., 2011; Kumar et al., 2012; Kumar et al., 2009; Watanabe et al., 2009), APC (Zhou et al., 2004), ACF7 (Wu et al., 2011), EB1 (Zhang et al., 2016). Here, we demonstrated that tyrosine residues within the TACC domain of TACC3 are important for maintaining the interaction between TACC3 and microtubules. The TACC domain with all tyrosine residues mutated into phenylalanine remains mostly cytoplasmic, while TACC wild-type localizes to microtubules. It should be noted that the wild-type TACC domain, in contrast to full-length TACC3 (which shows primarily plus-end binding), also showed lattice binding in addition to plus-end localization. Consistent with our previous observations (Nwagbara et al., 2014), this suggest that N-terminus of TACC3 is important for restricting TACC3 localization to the microtubule plus-ends.

+TIPs track microtubule plus-ends either autonomously, through recognition of the growing microtubule structure, or non-autonomously, through an interaction with another plus-end tracking protein such as end-binding (EB) proteins. Although the mechanism of how TACC3 tracks plus-ends is not fully resolved, EB-dependent plus-end tracking can be ruled out as TACC3 does not contain a SxIP motif (serine- any amino acid- isoleucine-proline) that is required for EB binding. It is believed that TACC3 tracks microtubule plus-ends through its interaction with XMAP215, which is mediated by the TACC domain (Kinoshita et al., 2005; Mortuza et al., 2014; Peset et al., 2005). Therefore, it is possible that the impaired interaction between microtubules and TACC phospho-null mutant could be due to a change in TACC3's ability to interact with XMAP215.

The TACC domain consists of two coiled-coil domains, which means that the sequence follows heptad repeats. Presence of these coiled-coil domains are responsible for TACC3's oligomerization, which is important for TACC3's function and its interaction with XMAP215 (Mortuza et al., 2014; Thakur et al., 2014). Using Multicoil, a coiled-coil prediction program, we looked at whether tyrosine-to-phenylalanine mutations might have altered coiled-coil formation or dimerization of TACC domain. Based on this prediction, it seems as though the TACC phospho-null mutant is still likely able to dimerize and form a

coiled-coil (Supplementary Figure 9), suggesting that the interaction between XMAP215 and TACC phospho-null mutant might be retained.

Although *in silico* analysis suggests that switching from phosphorylatable tyrosine to non-phosphorylatable phenylalanine would not impact TACC3's coiled-coil structure, reduced interaction between phospho-null TACC mutants and microtubules might be explained by a change in electrostatic interactions between the two. While this could be a possibility, negative charges introduced via phosphorylation often cause dissociation of proteins from the microtubule (Hur et al., 2011; Iimori et al., 2012) which is already loaded with negative charges due to negatively-charged residues at the C-terminus of tubulin. While our findings suggest that the tyrosine residues of TACC domain are important for mediating TACC3's interaction with microtubules, the exact mechanism of how they are involved in this interaction remains to be determined.

3.3 | TACC phospho-null mutant axons are shorter due to increased pausing and retraction

Our data showed that TACC phospho-null mutant-expressing axons of cultured neural tube explants were shorter in spite of slightly higher axon forward velocity rates compared to controls. When we further examined other axon outgrowth parameters, we found that TACC phospho-null mutants paused and retracted more frequently compared to TACC wild-type and controls (Figure 3d). Additionally, mutant axons grew with less directionality (Figure 3f).

In an attempt to seek further explanation to axon outgrowth behavior, we examined growth cone morphology, since growth cone morphology can predict or be a readout of the growth behavior of axon (Ren and Suter, 2016). For example, increased growth cone size is often associated with frequently pausing or slow growing axons. Although we did not see a significant difference in growth cone size, filopodia length, or number among conditions (Figure 4a-c), there was a significant increase in the number of filopodia with microtubules in the TACC-expressing growth cones. However, this increase was independent of TACC's phosphorylation status, as both TACC wild-type and TACC phospho-null mutant showed comparable increase in percent of filopodia with microtubules (Figure 4g).

It is known that microtubules can play an instructive role in growth cone directional motility. Having more filopodia with microtubules might generate more alternative routes for the growth cone to extend, which could result in more pausing for decision making and could also cause the growth cone to wander more, which would result in less directed movement. There might be increased and prolonged microtubule/F-actin coupling in TACC expressing growth cones, which would enable microtubules to track more persistently along F-actin into the filopodia. In fact, increased microtubule/F-actin coupling could also explain increased retraction rates. For example, actin filaments in the growth cone are subjected to rearward translocation also known as retrograde flow, due to myosin II activity (Suter and Forscher, 2000). The retrograde flow of actin filaments can be attenuated when the F-actin cytoskeleton engages with receptors at point contact sites. This interaction acts as a molecular clutch that would restrain actin retrograde flow, while continuing actin polymerization will generate the force to allow membrane protrusion, thereby growth cone

advance. The growth cone retracts when actin retrograde flow fails to be attenuated, which is also an indication of poor surface adhesion. It is known that dynamic microtubules play an important role in facilitating focal adhesion dynamics by transporting molecules that are involved in focal adhesion turnover (Stehbens and Wittmann, 2012). Several microtubule plus-end binding proteins have been studied for their association with adhesion sites (Stehbens et al., 2014; Zhang et al., 2016). Therefore, by facilitating microtubule protrusion into the filopodia, the TACC domain might be playing an indirect a role in adhesion dynamics.

A potential role in point contact regulation could also explain avoidance of EphrinA5-coated repellent substrates. Filopodia with microtubules could be more sensitive to cues, due to the microtubule-mediated signal trafficking, thereby affecting the interaction with the underlying substrate. Moreover, as speculated earlier, having more filopodia with microtubules could generate more alternative routes; thus, when the growth cone encounters a non-permissive substrate, it could pick one of these alternative routes and steer away from the repellent source.

Here, we have demonstrated that tyrosine residues within the TACC domain, which is the domain important for mediating microtubule plus-end tracking behavior, are critical for localizing the protein to microtubules and regulating axon outgrowth parameters. Given the increased number of microtubules in the filopodia when the TACC domain is over-expressed, we hypothesize that TACC domain might be involved in regulating a potential TACC-mediated interaction between microtubules and F-actin. Such an interaction has not been proposed for TACC3 before, however, there are studies that might offer a potential interaction between TACC3 and the actin cytoskeleton. A proteomic screen previously identified an interaction between TACC3 and actin regulator proteins Ena/VASP (Hubner et al., 2010). Additionally, the close interactor of TACC3, XMAP215, has recently been shown to interact with F-actin and mediate microtubule/F-actin interaction in growth cones (Slater et al., 2019), which makes TACC3 a candidate to be involved in actin cytoskeleton interaction either direct or indirectly.

To our knowledge, TACC3 tyrosine phosphorylation has not been explored extensively before. Nelson *et. al.* identified two tyrosine residues, Y684 and Y753 (corresponding to residues Y725 and Y832 in *Xenopus laevis* and conserved across species, Supplementary Figure 10) that showed enhanced phosphorylation when it is fused to Fibroblast Growth Factor Receptor 3 (FGFR3) (Nelson et al., 2016). It has been indicated that the FGFR3–TACC3 fusion is important for the activation of FGFR3 tyrosine kinase activity, and fusion of these proteins increases cell proliferation and tumor formation. Moreover, FGFR3-TACC3 fusion has been shown to pull TACC3 away from mitotic spindles and localize to the spindle poles, causing mitotic defects (Sarkar et al., 2017). From this perspective, it might be intriguing to investigate TACC domain tyrosine residues and association of TACC3 with microtubules during cell division.

Finally, in addition to tyrosine phosphorylation, serine/threonine phosphorylation sites within TACC3 would be worthwhile to explore in the future. There are several S/T kinases that operate under guidance cues, such as GSK3, which is a well-studied S/T kinase that is

already shown to phosphorylate various +TIPs and modulate microtubule dynamics. Future work can further explore whether TACC3 is targeted by S/T kinases and whether S/T phosphorylation would affect TACC3's function in a similar way, which could shed light on differential and asymmetric regulation of microtubule dynamics under various guidance signals.

4 | MATERIALS AND METHODS

4. 1 | Embryos

Eggs collected from *Xenopus laevis* were fertilized *in vitro* and kept between at 13-22°C in 0.1X Marc's Modified Ringer's (MMR). All experiments were approved by the Boston College Institutional Animal Care and Use Committee and were performed according to national regulatory standards.

4.2 | Culture of embryonic explants

Neural tubes of embryos staged according to Nieuwkoop and Faber were dissected at stages between 20-21 as described previously (Lowery et al., 2012). Neural tube explants were cultured on MatTek glass bottom dishes coated with poly-L-lysine (100 μg/ml) and laminin (20 μg/ml). Culture media prepared by mixing L-15 Leibovitz medium and Ringer's solution supplemented with antibiotics NT3 and BDNF to promote neurite outgrowth.

4.3 | Constructs and RNA

Capped mRNAs were transcribed and purified as previously described (Lowery et al., 2013; Nwagbara et al., 2014). TACC3 pET30a was a gift from the Richter lab, University of Massachusetts Medical School, Worcester, MA and sub-cloned into GFP pCS2+. Tyrosine phospho-null mutations were introduced into wild-type GFP-TACC3 by using overlapping extension PCR method with appropriate primers designed to substitute tyrosine residues with phenylalanine to generate GFP-TACC3 6xYF. Wild-type and phospho-null mutants of TACC domain were cloned from their full-length counterparts. MACF 43 (a gift from Hoogenraad Lab) was sub-cloned into mKate2 pCS2+. Embryos either at the 2-cell or 4-cell stage were injected with the following total mRNA amount per embryo; 100pg of GFP-MACF43 as a control for GFP-TACC3 and to analyze microtubule dynamics parameters. GFP-TACC3 full-length wild-type or phospho-null mutant injected at 1000 pg. GFP-TACC wild-type or phospho-null mutant were injected at 400pg. The human c-Abl construct was originally constructed in the Kufe lab (Harvard Medical School) (Cao et al. 2003) and gifted by Dr. Alan Howe (University of Vermont). The Fyn construct in pRK5-Entry (Mariotti et al. 2001) was acquired from AddGene (Cambridge, MA, USA).

4.4 | Cell Culture and Transfections

HEK293 cells were maintained at 37 °C and 5% CO_2 and cultured in DMEM containing L-glutamine, sodium pyruvate and 4.5 g/L glucose (MediaTech/Corning Life Sciences, Tewksbury, MA, USA). DMEM was supplemented with 5% fetal bovine serum (Hyclone, Logan, UT, USA), 5% Cosmic calf serum (Hyclone), 50 units/mL penicillin and 50μg/mL streptomycin (Penicillin-Streptomycin, Invitrogen, Carlsbad, CA, USA). Cells were cultured to 75% of confluence and transfected with 3-6μg GFP-TACC3 full-length (FL) with or

without 2μg c-Abl or 3.5μg Fyn expression plasmids using calcium phosphate precipitation. The following expression constructs encoding TACC3 phospho-null and truncation mutants were co-transfected at 3 μg with c-Abl: GFP-TACC3 Y2A (Y608A, Y628A); GFP-TACC3 Y3A (Y608A, Y628A, Y759A); GFP-TACC3 Y4A (Y608A, Y628A, Y759A, Y762A). GFP-TACC domain widtype; GFP-TACC domain phospho-null mutant (Y725F, Y759F, Y762F, Y832F, Y846F, Y857F).

4.5 | Cell Lysis, Immunoprecipitation and Western Blotting

HEK293 cells were lysed as previously described (St. Clair et al. 2019) in lysis buffer (25mM Tris pH 7.4, 137mM NaCl, 10% glycerol, 1% Igepal) containing protease inhibitors (5μg/mL Pepstatin, 10μg/mL Leupeptin, 1mM PMSF) and phosphatase inhibitors (1mM $NaVO_3$, 25 mM NaF, 10mM $Na_2H_2P_2O_7$). For cell extract immunoblotting, 20-30μg total protein extract was denatured in protein sample buffer (125mM Tris pH 6.8, 7.5% glycerol, 2% sodium dodecyl sulfate (SDS), 5% β-mercaptoethanol, and 0.02% bromophenol blue) at 95 °C for 5 minutes and subjected to SDS-PAGE. For immunoprecipitation experiments, 1000μg of total protein was incubated overnight at 4 °C with 2μg α-GFP (Life Technologies/ ThermoFisher Scientific, Carlsbad, CA, USA) and 20μL of a 50% slurry of sepharose Protein A (Rockland Immunochemicals, Limerick, PA, USA) and Protein G resin (G-Biosciences, St. Louis, MO, USA) prewashed with lysis buffer. Immune complexes were washed 3 times with lysis buffer, dried and denatured in protein sample buffer at 95 °C for 5 minutes. Denatured cell extract and immunoprecipitation samples were subjected to SDS-PAGE separation. For mass spectrometry analysis, the SDS-PAGE gel was stained with Coomassie (0.1% Coomassie brilliant blue R-250, 20% glacial acetic acid and 40% methanol) and subsequently prepared for mass spectrometry as described below. For immunoblotting experiments, the following primary antibodies were diluted in 10 mL of 1.5% BSA in TBST containing 0.0005% sodium azide and incubated at 4 °C with the membranes overnight: α-GFP (1:2000, rabbit pAb, Life Technologies); α-Abl (1:1000, rabbit pAb, Santa Cruz Biotechnology, Dallas, TX, USA); α-phosphotyrosine 4G10 (1:1000, mouse mAb, EMD Millipore, Billerica, MA, USA). The following secondary antibodies were used: α-mouse-HRP (goat IgG, 1:5000; EMD Millipore); α-rabbit-HRP (goat IgG, 1:15,000, EMD Millipore); or for immunoprecipitation experiments, α-rabbit-HRP Light Chain Specific (goat IgG, 1:10,000, Jackson ImmunoResearch Laboratories, West Grove, PA, USA). Proteins were detected using enhanced chemiluminescence (ThermoFisher Scientific, Waltham, MA, USA) and film was developed using a Medical Film Processor SRX-101A (Konica Minolta Medical and Graphic, Tokyo, Japan).

4.6 | Mass Spectrometry

To identify Abl-induced phosphorylation sites on TACC3, GFP-TACC3 was transfected with or without c-Abl. GFP-TACC3 was immunoprecipitated using α-GFP and subjected to SDS-PAGE separation and Coomassie staining as described above. The region corresponding to the molecular weight of GFP-TACC3 (180 kDa) was excised and prepared for mass spectrometry as previously described (Cheerathodi et al. 2015). Briefly, gel regions were diced and proteins were subjected to in-gel digestion with 6ng/μL trypsin (Promega, Madison, WI, USA) in 50mM ammonium bicarbonate at 37 °C for 10-12 hours. The tryptic peptides were resuspended in 2.5% acetonitrile, 0.15% formic acid and separated via HPLC

prior to MS/MS analysis on a linear ion trap-orbitrap (LTQ-Orbitrap) mass spectrometer (Thermo Electron, Waltham, MA, USA) controlled with Thermo Xcalibur 2.1 software. Peptides were eluted and electrosprayed (2.1 kV) into the mass spectrometry as previously described (St. Clair et al. 2018). The precursor scan (scan range = 360-1700 *m/z*, resolution = 3.0×10^4) was followed by ten collision-induced dissociation (CID) tandom mass spectra. CID spectra were acquired for the top ten ions in the precursor scan.

A SEQUEST search of the mass spectrometry data was performed using the forward and reverse *Xenopus* TACC3 Uniprot sequence requiring tryptic peptides and permitting phosphorylation of serine, threonine and tyrosine (+79.9663 Da), oxidation of methionine (+15.9949 Da), and acrylamidation of cysteine (+71.0371Da). Peptides were identified with a false discovery rate of less than 1%.

4.7 | Immunocytochemistry

Embryonic explant cultures were fixed with 0.2% Glutaraldehyde as described (Challacombe et al., 1997) and labelled with primary antibody (1:1000 diluted in blocking buffer made up by 1% non-fat dry milk in calcium and magnesium free PBS) to tyrosinated tubulin [YL1/2] (rat monoclonal, ab6160, Abcam) for 45 min at room temperature which is followed by PBS washes repeated three times and 10 min of blocking. Goat anti-rat AlexaFluor568 (1:500, ab175476, Abcam Technologies) was used as a secondary to tubulin and Phalloidin 488 (1:500, Molecular Probes) was used to label actin. Both reagents are diluted in blocking solution and applied for 45 min at room temperature followed by PBS washes several times. 90% glycerol stock was used as a mounting media for imaging.

4.8 | Stripe Assay

The stripe assay is performed as described in Knoll et al 2007 (Knöll et al., 2007). 10μg/ml of Ephrin-A5/Fc (chimera human, Sigma, E0628) and 10μg/ml of Fc are mixed with 2.5μg/ml of Anti-human IgG (Fc specific) FITC (Sigma, F9512) and Anti-human IgG (Fc specific) respectively in PBS. Solutions are incubated at room temperature for 30 min to allow for oligomerization. To coat coverslips with Ephrin-A5, a coverslip is attached to a zig-zag patterned silicon matrix and Ephrin-A5 solution is injected with a micropipette through the channel in the silicon. Injected matrices are incubated at 37°C for 30 min and then rinsed with PBS several times using the same injection method. After rinsing, coverslips are detached from the matrix and placed in a culture dish and 100μl of second stripe solution (Fc only) is applied directly on the coverslip and incubated at 37°C for 30 min. After incubation is over coverslips are rinsed with PBS and 20μg / ml of 100ul laminin in PBS is applied on coverslips and incubated for 1 h. After laminin incubation coverslips are rinsed with PBS several times. 400μl of culture media is applied on coverslips and neural tube explants are placed on protein coated area and cultured for 24 h prior to imaging.

4.9 | Image acquisition and analysis

To assess axon outgrowth parameters, phase contrast images of axons were collected on a Zeiss Axio Observer inverted motorized microscope with a Zeiss 20×/0.5 Plan Apo phase objective. For axon outgrowth length, snap-shots of neural tube explants were taken 12-18h post culturing. Time-lapse images were collected for 4 h with 5 min intervals and axon

growth was manually tracked frame by frame using Fiji Manual Tracking plugin. Axon growth velocity information is provided by the Manual Tracking plugin but only the forward movement velocity was included in the analysis. Axon outgrowth forward movement, pause and retraction frequencies (as a percentage of total frames tracked) are scored manually tracking axons frame by frame.

High-resolution images of cultured spinal cord explants were obtained with a CSU-X1M 5000 spinning-disk confocal (Yokogawa) on a Zeiss Axio Observer inverted motorized microscope with a Zeiss Plan-Apochromat 63×/1.40 numerical aperture lens. Images were acquired with an ORCA R2 charge-coupled device camera (Hamamatsu) controlled with Zen software. For microtubule dynamics and TACC localization experiments, images are time lapse images are acquired for 1 min with 2 s intervals.

Structured illumination super-resolution images were collected on a Zeiss Axio Observer.Z1 for super-resolution microscope with Elyra S.1 system, utilizing an Objective Plan-Apochromat 63×/1.40 oil (DIC). Images were acquired with a PCO-Tech Inc.pco.edge 4.2 sCMOS camera. The images were obtained in a chamber at approximately 28°C and utilizing the immersion oil Immersol 518F 30°. Channel alignment and structured illumination processing were applied to the super-resolution images using the Zeiss Black program. Experiments were performed multiple times to ensure reproducibility. Graphs were made in GraphPad Prism. Statistical differences were determined using unpaired two tailed t-tests when comparing two conditions and one-way analysis of variance (ANOVA) with Tukey's *post-hoc* analysis when multiple conditions were compared.

Supplementary Material

Refer to Web version on PubMed Central for supplementary material.

Acknowledgements

We thank members of the Lowery Lab for helpful discussions, suggestions, and editing, especially Sangmook Lee, Paula Slater, Beth Bearce and Micaela Lasser. We thank Nancy McGilloway and Todd Gaines for excellent *Xenopus* husbandry. We also thank the National *Xenopus* Resource (RRID:SCR013731) and Xenbase (RRID:SCR-003280) for their support. We thank Bret Judson and the Boston College Imaging Core for infrastructure and support. This work was supported by NIH/NIMH (MH109651) to LAL, National Science Foundation IOS award 1656510 to BB, National Institutes of Health grant 8P20GM103449 (Vermont Genetics Network/ Vermont INBRE program) to BB, and National Science Foundation (Grant No. 1626072). The authors have no conflicts of interest. The data that support the findings of this study are available from the corresponding author upon request.

REFERENCES

Bearce EA, Erdogan B, and Lowery LA. 2015 TIPsy tour guides: how microtubule plus-end tracking proteins (+TIPs) facilitate axon guidance. Front Cell Neurosci. 9:241. [PubMed: 26175669]

Buck KB, and Zheng JQ. 2002 Growth cone turning induced by direct local modification of microtubule dynamics. J Neurosci. 22:9358–9367. [PubMed: 12417661]

Challacombe JF, Snow DM, and Letourneau PC. 1997 Dynamic microtubule ends are required for growth cone turning to avoid an inhibitory guidance cue. J Neurosci. 17:3085–3095. [PubMed: 9096143]

Engel U, Zhan Y, Long JB, Boyle SN, Ballif BA, Dorey K, Gygi SP, Koleske AJ, and Vanvactor D. 2014 Abelson phosphorylation of CLASP2 modulates its association with microtubules and actin. Cytoskeleton (Hoboken). 71:195–209. [PubMed: 24520051]

Erdogan B, Cammarata GM, Lee EJ, Pratt BC, Francl AF, Rutherford EL, and Lowery LA. 2017 The microtubule plus-end-tracking protein TACC3 promotes persistent axon outgrowth and mediates responses to axon guidance signals during development. Neural Dev. 12:3. [PubMed: 28202041]

Hubner NC, Bird AW, Cox J, Splettstoesser B, Bandilla P, Poser I, Hyman A, and Mann M. 2010 Quantitative proteomics combined with BAC TransgeneOmics reveals in vivo protein interactions. J Cell Biol. 189:739–754. [PubMed: 20479470]

Hur EM, Saijilafu BD Lee, Kim SJ, Xu WL, and Zhou FQ. 2011 GSK3 controls axon growth via CLASP-mediated regulation of growth cone microtubules. Genes Dev. 25:1968–1981. [PubMed: 21937714]

Iimori M, Ozaki K, Chikashige Y, Habu T, Hiraoka Y, Maki T, Hayashi I, Obuse C, and Matsumoto T. 2012 A mutation of the fission yeast EB1 overcomes negative regulation by phosphorylation and stabilizes microtubules. Exp Cell Res. 318:262–275. [PubMed: 22134091]

Kinoshita K, Noetzel TL, Pelletier L, Mechtler K, Drechsel DN, Schwager A, Lee M, Raff JW, and Hyman AA. 2005 Aurora A phosphorylation of TACC3/maskin is required for centrosome-dependent microtubule assembly in mitosis. The Journal of cell biology. 170:1047–1055. [PubMed: 16172205]

Knöll B, Weinl C, Nordheim A, and Bonhoeffer F. 2007 Stripe assay to examine axonal guidance and cell migration. Nat Protoc. 2:1216–1224. [PubMed: 17546017]

Kumar P, Chimenti MS, Pemble H, Schönichen A, Thompson O, Jacobson MP, and Wittmann T. 2012 Multisite phosphorylation disrupts arginine-glutamate salt bridge networks required for binding of cytoplasmic linker-associated protein 2 (CLASP2) to end-binding protein 1 (EB1). J Biol Chem. 287:17050–17064. [PubMed: 22467876]

Kumar P, Lyle KS, Gierke S, Matov A, Danuser G, and Wittmann T. 2009 GSK3beta phosphorylation modulates CLASP-microtubule association and lamella microtubule attachment. J Cell Biol. 184:895–908. [PubMed: 19289791]

Lee H, Engel U, Rusch J, Scherrer S, Sheard K, and Van Vactor D. 2004 The microtubule plus end tracking protein orbit/MAST/CLASP acts downstream of the tyrosine kinase Abl in mediating axon guidance. Neuron. 42:913–926. [PubMed: 15207236]

Lee MJ, Gergely F, Jeffers K, Peak-Chew SY, and Raff JW. 2001 Msps/XMAP215 interacts with the centrosomal protein D-TACC to regulate microtubule behaviour. Nat Cell Biol. 3:643–649. [PubMed: 11433296]

Lowery LA, Faris AE, Stout A, and Van Vactor D. 2012 Neural Explant Cultures from Xenopus laevis. J Vis Exp:e4232. [PubMed: 23295240]

Lowery LA, Lee H, Lu C, Murphy R, Obar RA, Zhai B, Schedl M, Van Vactor D, and Zhan Y. 2010 Parallel genetic and proteomic screens identify Msps as a CLASP-Abl pathway interactor in Drosophila. Genetics. 185:1311–1325. [PubMed: 20498300]

Lowery LA, Stout A, Faris AE, Ding L, Baird MA, Davidson MW, Danuser G, and Van Vactor D. 2013 Growth cone-specific functions of XMAP215 in restricting microtubule dynamics and promoting axonal outgrowth. Neural development. 8:22. [PubMed: 24289819]

Lowery LA, and Van Vactor D. 2009 The trip of the tip: understanding the growth cone machinery. Nature reviews. Molecular cell biology. 10:332–343. [PubMed: 19373241]

Mortuza GB, Cavazza T, Garcia-Mayoral MF, Hermida D, Peset I, Pedrero JG, Merino N, Blanco FJ, Lyngso J, Bruix M, Pedersen JS, Vernos I, and Montoya G. 2014 XTACC3-XMAP215 association reveals an asymmetric interaction promoting microtubule elongation. Nature communications. 5:5072.

Nelson KN, Meyer AN, Siari A, Campos AR, Motamedchaboki K, and Donoghue DJ. 2016 Oncogenic Gene Fusion FGFR3-TACC3 Is Regulated by Tyrosine Phosphorylation. Mol Cancer Res. 14:458–469. [PubMed: 26869289]

Nwagbara BU, Faris AE, Bearce EA, Erdogan B, Ebbert PT, Evans MF, Rutherford EL, Enzenbacher TB, and Lowery LA. 2014 TACC3 is a microtubule plus end-tracking protein that promotes axon

elongation and also regulates microtubule plus end dynamics in multiple embryonic cell types. Mol Biol Cell. 25:3350–3362. [PubMed: 25187649]

Peset I, Seiler J, Sardon T, Bejarano LA, Rybina S, and Vernos I. 2005 Function and regulation of Maskin, a TACC family protein, in microtubule growth during mitosis. The Journal of cell biology. 170:1057–1066. [PubMed: 16172207]

Peset I, and Vernos I. 2008 The TACC proteins: TACC-ling microtubule dynamics and centrosome function. Trends in cell biology. 18:379–388. [PubMed: 18656360]

Ren Y, and Suter DM. 2016 Increase in Growth Cone Size Correlates with Decrease in Neurite Growth Rate. Neural Plast. 2016:3497901. [PubMed: 27274874]

Sarkar S, Ryan EL, and Royle SJ. 2017 FGFR3-TACC3 cancer gene fusions cause mitotic defects by removal of endogenous TACC3 from the mitotic spindle. Open Biol. 7.

Slater PG, Cammarata GM, Samuelson AG, Magee A, Hu Y, and Lowery LA. 2019 XMAP215 promotes microtubule-F-actin interactions to regulate growth cone microtubules during axon guidance in. J Cell Sci. 132.

Stehbens S, and Wittmann T. 2012 Targeting and transport: How microtubules control focal adhesion dynamics. Journal of Cell Biology. 198:481–489.

Stehbens SJ, Paszek M, Pemble H, Ettinger A, Gierke S, and Wittmann T. 2014 CLASPs link focal-adhesion-associated microtubule capture to localized exocytosis and adhesion site turnover. Nat Cell Biol. 16:561–573. [PubMed: 24859005]

Suter DM, and Forscher P. 2000 Substrate-cytoskeletal coupling as a mechanism for the regulation of growth cone motility and guidance. J Neurobiol. 44:97–113. [PubMed: 10934315]

Thakur HC, Singh M, Nagel-Steger L, Kremer J, Prumbaum D, Fansa EK, Ezzahoini H, Nouri K, Gremer L, Abts A, Schmitt L, Raunser S, Ahmadian MR, and Piekorz RP. 2014 The centrosomal adaptor TACC3 and the microtubule polymerase chTOG interact via defined C-terminal subdomains in an Aurora-A kinase-independent manner. J Biol Chem. 289:74–88. [PubMed: 24273164]

Watanabe T, Noritake J, Kakeno M, Matsui T, Harada T, Wang S, Itoh N, Sato K, Matsuzawa K, Iwamatsu A, Galjart N, and Kaibuchi K. 2009 Phosphorylation of CLASP2 by GSK-3beta regulates its interaction with IQGAP1, EB1 and microtubules. J Cell Sci. 122:2969–2979. [PubMed: 19638411]

Wittmann T, and Waterman-Storer CM. 2005 Spatial regulation of CLASP affinity for microtubules by Rac1 and GSK3beta in migrating epithelial cells. J Cell Biol. 169:929–939. [PubMed: 15955847]

Wu X, Shen QT, Oristian DS, Lu CP, Zheng Q, Wang HW, and Fuchs E. 2011 Skin stem cells orchestrate directional migration by regulating microtubule-ACF7 connections through GSK3β. Cell. 144:341–352. [PubMed: 21295697]

Zhang Y, Luo Y, Lyu R, Chen J, Liu R, Li D, Liu M, and Zhou J. 2016 Proto-Oncogenic Src Phosphorylates EB1 to Regulate the Microtubule-Focal Adhesion Crosstalk and Stimulate Cell Migration. Theranostics. 6:2129–2140. [PubMed: 27698945]

Zhou FQ, Zhou J, Dedhar S, Wu YH, and Snider WD. 2004 NGF-induced axon growth is mediated by localized inactivation of GSK-3beta and functions of the microtubule plus end binding protein APC. Neuron. 42:897–912. [PubMed: 15207235]

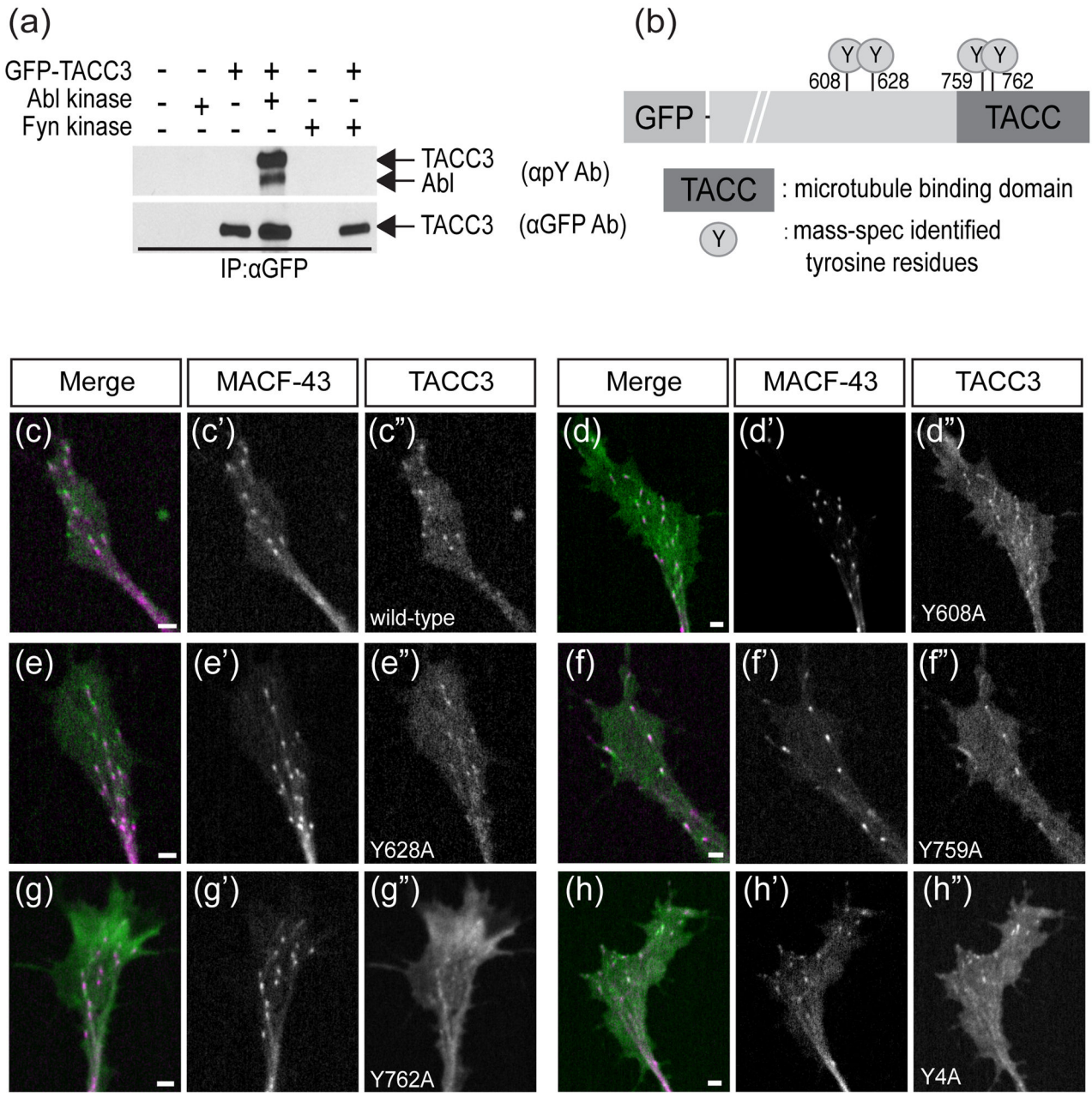

FIGURE 1.

Abelson kinase induces phosphorylation of TACC3 Abelson kinase induces phosphorylation of TACC3. (a) Western blot performed with phospho-tyrosine specific antibody showing Abelson-induced tyrosine phosphorylation of full-length TACC3 (lane 4). Phosphorylation signal is not present when TACC3 is expressed alone (lane 2) or with another tyrosine kinase Fyn (lane 6). (b) Cartoon showing mass-spec-identified tyrosine residues of TACC3 targeted by Abl phosphorylation. (c-h) Confocal images of growth cones expressing MACF-43 (magenta) and TACC3 (green) with phospho-null mutations at identified residues, showing localization of TACC3 phospho-null mutants to microtubule plus-ends. Scale bar, 2μm.

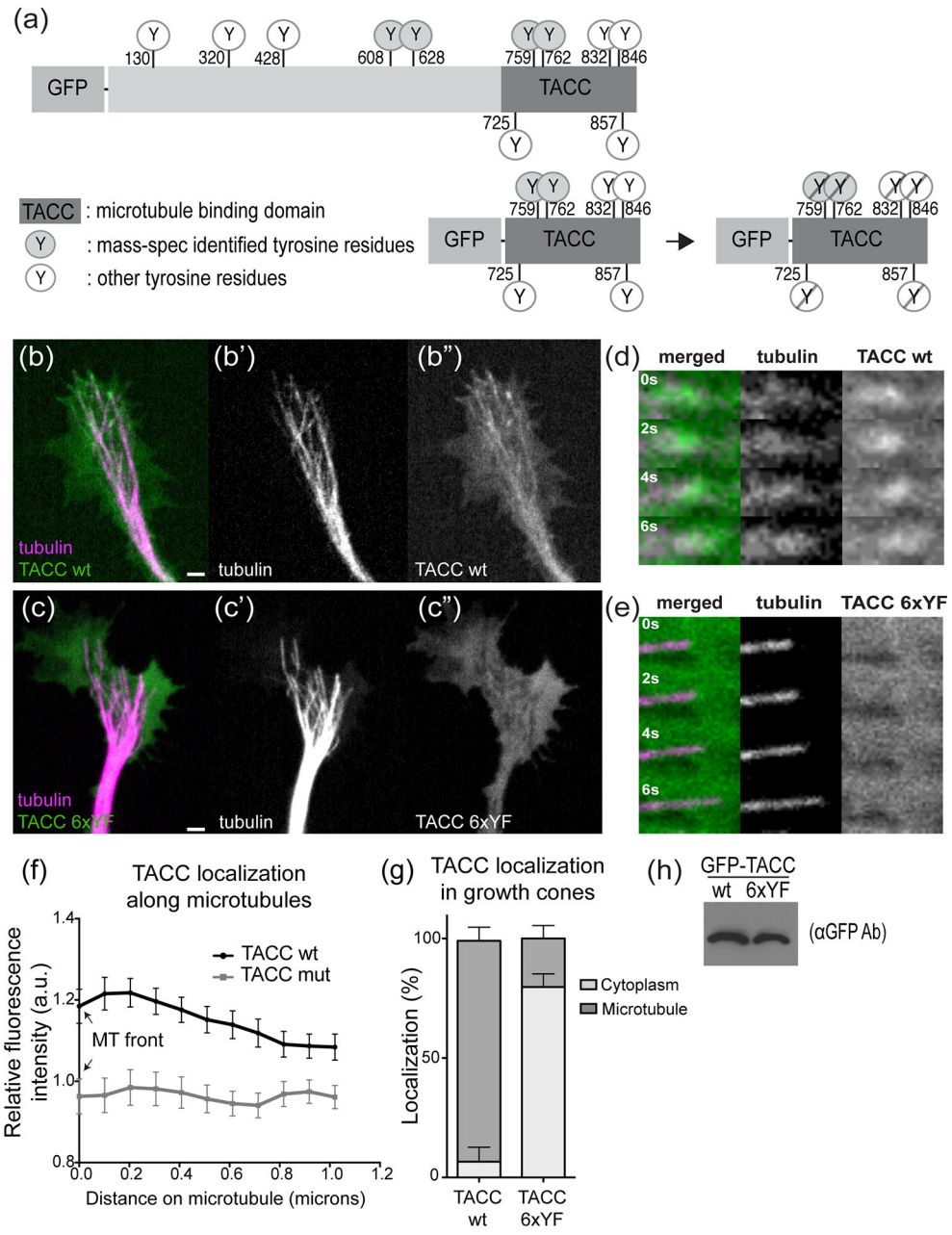

FIGURE 2.

Tyrosine phospho-null mutations impair the localization of TACC domain at microtubule plus-ends in growth cones and mesenchymal cells. (a) Cartoon showing mass-spec-identified tyrosine residues and other tyrosine residues of TACC3 (top) and the TACC domain with residues mutated to phenylalanine in the GFP-TACC phospho-null 6xYF construct. (b-c) Confocal images of neuronal growth cones, obtained from time-lapse recordings expressing tubulin (magenta) (b', c') and TACC (green) wild-type (b") or tyrosine phospho-null mutant (c"). (d-e) Magnified montages of time-lapse sequences of single microtubule. TACC wild-type (green) localizes to microtubule (magenta) plus-ends (d) while TACC tyrosine phospho-null mutant (green) is absent from microtubule (magenta) plus-ends and remains

mostly cytoplasmic (e). (f) Fluorescent intensity profile (y-axis) along microtubules (x-axis) determined by line-scan analysis showing green fluorescent intensity (TACC wt or TACC p-null mutant) relative to background. Line is drawn starting from the beginning of the microtubule plus-end. (g) Plot showing the quantification of microtubule plus-end versus cytoplasmic localization of TACC constructs within the growth cones as percentage of total growth cones examined. On average, TACC wild-type shows microtubule plus-end binding in 92.5% of the growth cones examined while TACC tyrosine p-null mutant showed plus-end localization in 20% of the growth cones and remained mostly cytoplasmic in 80% of the growth cones examined. (h) Western blot performed with GFP antibody showing the expression of GFP-TACC wild-type and GFP-TACC phospho-null mutant. Scale bar, 2μm.

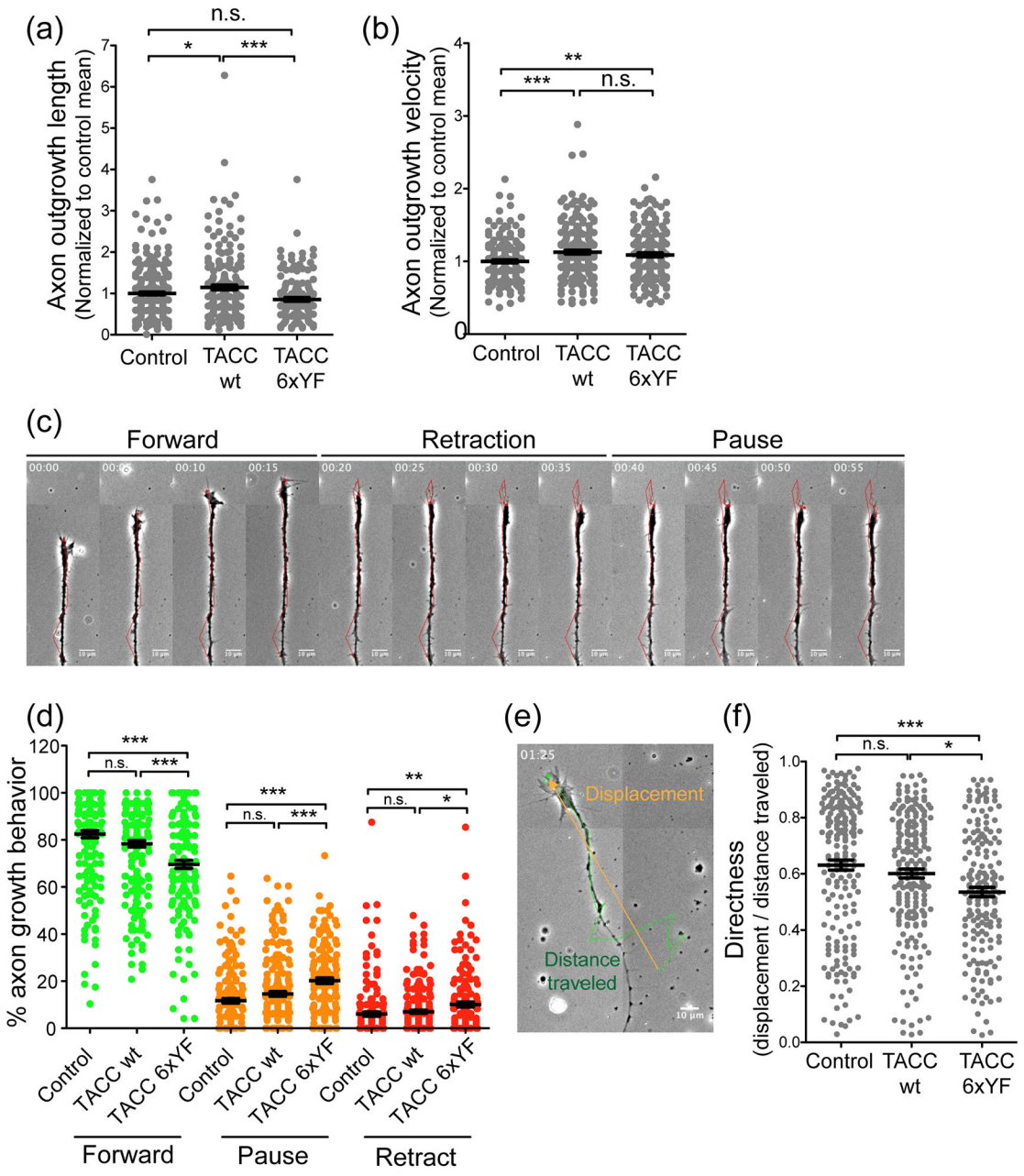

FIGURE 3.

TACC tyrosine phospho-null mutant expressing axons grow less persistently thereby grow shorter axons compared to TACC wt axons. (a) Quantification of axon length in cultured neural tube explants shows TACC phospho-null mutant expressing neurons grow axons shorter by 16.8% compared to control and 34% compared to TACC wt, while TACC wt expressing explants grow axons longer by 12.8% compared to control. (b) Measurement of axon forward movement velocity showing TACC wt increases axon forward movement velocity by 10% compared to control while TACC phospho-null mutant increases by 8%. (c) Representative phase contrast image montage of an axon depicting phases of forward movement, retraction and pause. (d) Plot showing the percentage of forward movement

(green), pause (orange) and retraction (red) of axon growth. TACC phospho-null mutant expressing axons spend 18% less time moving forward compared to control and 12% compared to TACC wt (green dots). TACC phospho-null mutant axons (20.20 ± 1.150 N=168) spent 42% more time pausing compared to control and 27% compared to TACC wt (orange dots). They also retract more frequently; 39% compared to control and 30% compared to TACC wt. (e) Representative image of an axon growth track depicting displacement and distance traveled between t=0 and t=1h 25min (f) Plot showing the directness of axon growth. TACC phospho-null mutant axons grow 12% less directly compared to TACC wt) and 17% compared to control axons. TACC wt axons also grow 5% less directly compared to control but it was not significant. The asterisk (*) indicates statistical significance with * $p < 0.05$, ** $p < 0.01$, *** $p < 0.001$, n.s. indicates not significant, from an ANOVA analysis comparing multiple conditions with Tukey's post hoc analysis. Values given are mean of normalized data pooled from independent experiments. The asterisk (*) indicates statistical significance with * $p < 0.05$, ** $p < 0.01$, *** $p < 0.001$, n.s. indicates not significant.

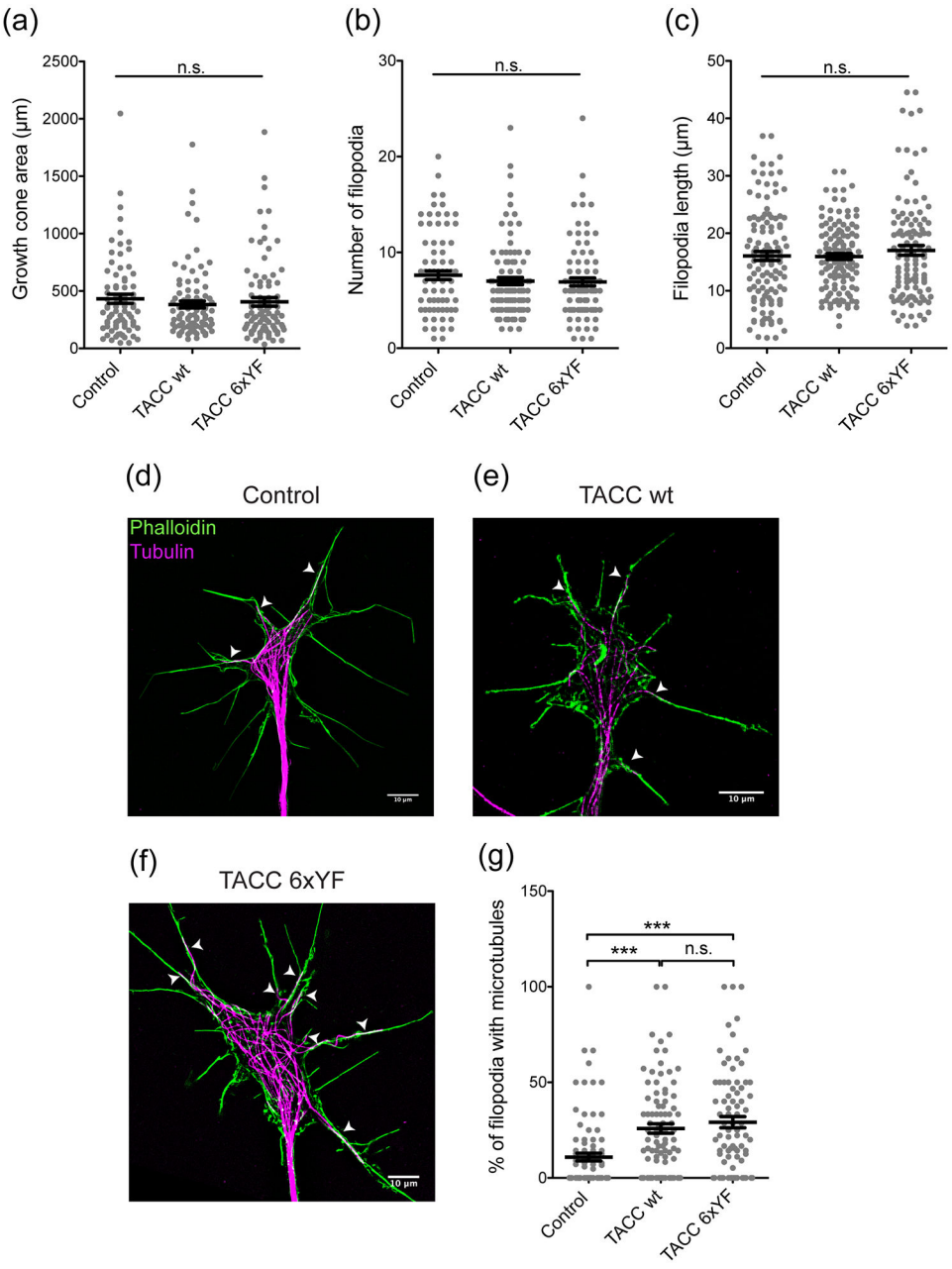

FIGURE 4.

TACC tyrosine phospho-null mutant-expressing growth cones display increased numbers of filopodia that contain microtubules. (a-c) The average growth cone area of TACC mutant (406.5 ± 37.17 µm, N=88) expressing growth cones was 13% smaller than control (432.6 ± 39.62 µm, N=77) and 6% larger than TACC wt (382.5 ± 30.17 µm, N=94) (a). TACC p-null mutant growth cones had an average of 6.9 ± 0.4130 N=93 filopodia which was 10% less than control growth cones (7.6 ± 0.4510 N=89) while TACC wt had 9% fewer filopodia than control (7.0 ± 0.3812 N=101) (b). The average filopodia length in TACC p-null mutant growth cones was 17.03 ± 0.8448µm, N=113, while it was 16.07 ± 0.7707 µm, N=119 in control growth cones, and 15.96 ± 0.5079 µm, N=126 in TACC wt expressing growth cones

(c). (d-f) Representative SIM images of control (d), TACC wt (e) and TACC phospho-null mutant (6xYF) (f) growth cones. (g) Quantification of the percentage of filopodia with microtubules. Almost 30% of the filopodia had microtubules in the TACC p-null mutant growth cones (29.13 ± 2.932 percent of total filopodia examined, N=82), which is 63% more than control growth cones (10.92 ± 2.011 percent of total filopodia examined, N=90), that had only 11% of their filopodia invaded by microtubules. TACC wt-expressing growth cones also had a greater number of filopodia with microtubules (25.82 ± 2.446 N=92) compared to controls. While not significant, TACC p-null growth cones had 11% more filopodia with microtubules compared to TACC wt. Scale bar 10μm. The asterisk (*) indicates statistical significance with * $p < 0.05$, ** $p < 0.01$, *** $p < 0.001$, n.s. indicates not significant.

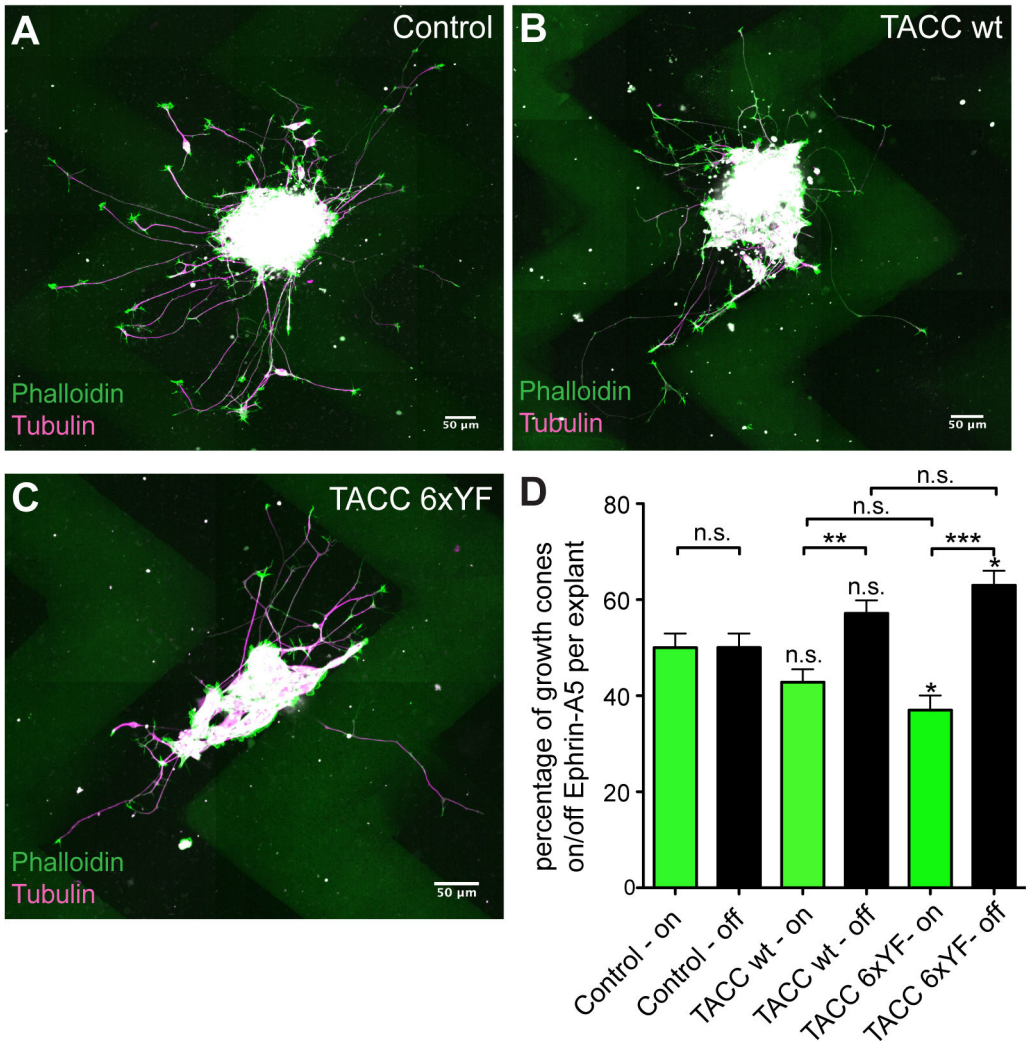

FIGURE 5.

TACC tyrosine phospho-null mutant-expressing axons are more responsive to repellent guidance signals. (a-c) Immunofluorescence images of control (a). TACC wt (b) and TACC p-null mut (c) labelled with phalloidin (green) to label growth cones and tubulin (red) to label axons showing axon responsiveness to Ephrin-A5 coated zigzag surfaces (green). (d) Quantification of the number of axons on permissive (Ephrin-A5 free) versus non-permissive (Ephrin-A5) surfaces. Control neural tube explants does not show a preference between permissive versus non-permissive surfaces and grow axons on both surfaces equally (Control - off, 50.01 ± 2.930 N=55; Control- on, 49.99 ± 2.930, respectively). TACC wt expressing neural tube explants grow 25% more axons on permissive surfaces (TACC wt – off, 57.18 ± 2.683 N=62), compared to Ephrin-A5 coated surface (TACC wt - on, 42.82 ± 2.683 N=62). TACC p-null mutants grow 41.3% more axons on permissive surface (TACC mut - off,63.02 ± 3.036 N=42) compared to Ephrin-A5 coated non-permissive surface (TACC mut - on, 36.98 ± 3.036 N=42). N, is the number of explants examined. Scale bar 50µm. The asterisk (*) indicates statistical significance with * $p < 0.05$, ** $p < 0.01$, *** $p <$

0.001, n.s. indicates not significant. t- test is used to compare two conditions, error bars indicate ± SEM.